

Bounding LVR in AMMs via Secant–Tangent Divergence and Collateralized Liquidity Scaling

Hyongsung Kim  

Korea Electronics Technology Institute, Republic of Korea

Yong-Suk Park¹  

Korea Electronics Technology Institute, Republic of Korea

Abstract

Automated Market Makers face a geometric dilemma: expanding liquidity depth to reduce execution slippage increases Liquidity Providers’ exposure to toxic arbitrage, quantified as Loss-Versus-Rebalancing (LVR). We study the Hybrid Liquidity-Collateral Pool (HLCP), a stylized architecture that aims to partially decouple execution quality from active risk exposure through an N -scaled virtual invariant and a collateral buffer. The analysis first characterizes the geometric divergence between execution slippage and marginal-price deviation, then uses this divergence to motivate a trigger-based collateral injection rule. In a stylized duopoly model, under hyper-saturated background liquidity and non-zero volatility or collateral yield, adopting the HLCP is a Nash equilibrium and Pareto-improving relative to a standard AMM benchmark. Empirically, we examine two settings. Under a stochastic-volatility-with-jumps stress scenario, the trigger policy avoids one-shot total buffer depletion under the imposed control law and simulated shock path. Using 2025 Uniswap V2 data with zero collateral yield, the HLCP exhibits lower realized LVR and higher net LP return than the standard CPMM benchmark in the sample considered.

2012 ACM Subject Classification Applied computing → Economics

Keywords and phrases Adverse Selection, Automated Market Maker, Capital Efficiency, Decentralized Finance, Liquidity Provision, Loss-Versus-Rebalancing

Digital Object Identifier 10.4230/LIPIcs.CVIT.2016.23

Acknowledgements This work was supported by the Institute of Information & Communications Technology Planning & Evaluation(IITP) grant funded by the Korea government(MSIT) (No.RS-2026-25507979, AI Data Training Verification and Reliability Assurance Technology)

1 Introduction

The emergence of Automated Market Makers (AMMs) based on the Constant Product Market Maker (CPMM) model [10], defined by the invariant $x \cdot y = k$, has revolutionized Decentralized Finance (DeFi). Despite their success, these protocols suffer from an economic vulnerability: Loss-Versus-Rebalancing (LVR), which transforms ‘Impermanent Loss (IL)’ into a permanent depletion of capital [5, 11, 12, 15]. While IL is an opportunity cost incurred when asset prices diverge, it is reversible if prices mean-revert. However, because AMMs lack access to external oracles, their internal price discovery lags behind Centralized Exchanges (CEXs). This information asymmetry creates an arbitrage gap. Arbitrageurs exploit stale on-chain prices to extract appreciating assets, maintaining the k invariant at the expense of the liquidity provider’s (LP) wealth. Consequently, the combination of directional market risk and counterparty intermediation costs ensures the LP’s position value remains inferior to a ‘buy-and-hold’ benchmark, even if prices revert. Mitigating LVR requires reducing liquidity exposure within the AMM. However, lower exposed capital also reduces depth,

¹ corresponding author



increases slippage, and can weaken fee generation. This creates a liquidity-depth trade-off: protecting LPs from adverse selection can make the pool less attractive to order flow. The design problem is therefore to improve this trade-off, rather than to eliminate it entirely.

In this paper, we study the Hybrid Liquidity-Collateral Pool (HLCP), a stylized architecture that places part of total capital in a collateral buffer while exposing only a calibrated active fraction through an N -scaling mechanism. The motivating observation is a saturation effect: beyond a threshold, additional liquidity yields only limited slippage improvement while continuing to increase LP exposure to LVR. The execution claim is therefore not literal identity with a full-reserve pool, but a tolerance-bounded approximation in saturated markets, developed later in Section 4.3. To react to stress without leaving all capital continuously on the active curve, the HLCP uses an endogenous kinetic trigger based on marginal-price deviations. When the deviation becomes economically meaningful, collateral is injected in a price-ratio-preserving step. At the implementation level, this mechanism requires only transaction-local state synchronization; a full gas-cost analysis is outside the scope of the present paper.

Our contributions are as follows:

- **Theory of Liquidity Saturation:** We characterize the divergence between execution slippage and marginal-price deviation, identifying a saturation region in which further physical liquidity delivers sharply diminishing execution benefits while preserving LVR exposure.
- **HLCP Architecture and Kinetic Trigger:** We introduce an N -scaled active pool together with a collateral buffer and specify a trigger-based collateral deployment rule driven by marginal-price deviations.
- **Stress-Path Validation under SVJ Dynamics:** We implement a stochastic-volatility-with-jumps (SVJ) [3] stress experiment at 12-second block resolution. The experiment is used to test whether the imposed control rule remains bounded away from one-shot total buffer depletion under an explicitly adverse shock path.
- **Historical Backtest of Net LP Outcomes:** Using 2025 Uniswap V2 data, we evaluate net LP performance under the conservative assumption $Y_C(T) = 0$. Under the stylized routing assumption of Section 4.3, the HLCP exhibits lower realized LVR and higher net LP return than the standard CPMM benchmark on the sample path considered.

The remainder of this paper is structured as follows. Section 2 reviews CPMM mechanics and formalizes LVR. Section 3 analyzes the incentive-compatibility trilemma and limitations of existing mitigations. Section 4 introduces the HLCP architecture, the N -scaling mechanism, and the kinetic trigger. Section 5 presents the two empirical evaluations: micro-resilience under SVJ stress and long-horizon historical profitability. Section 6 concludes the paper.

2 Background and Related Dynamics

This section establishes the theoretical foundation of structural vulnerabilities in Decentralized Exchanges (DEXs). Section 2.1 reviews CPMM mechanics and liquidity depth. Section 2.2 explains the limitations of Impermanent Loss (IL) and formalizes LVR as the path-dependent cost of adverse selection, framing the mathematical boundaries our proposed architecture seeks to overcome.

2.1 Constant Product Market Maker

An AMM algorithm minimizes slippage (price impact) by increasing liquidity depth. In the Constant Product Formula, the reserves of two assets, x and y , maintain a constant product k : $x \cdot y = k$. Following Uniswap conventions, liquidity is measured as $L = \sqrt{k}$, and any trade $(\Delta x, \Delta y)$ must preserve the invariant L^2 . However, this framework possesses an architectural limitation: algorithmic depth (L) is bound to physical reserves (x, y) . Consequently, compressing execution slippage requires an expansion of physical capital. This creates capital inefficiency, mandating that 100% of the LP's assets remain exposed to the active trading function and its adverse selection costs to maintain competitive execution pricing.

2.2 Impermanent Loss and Loss-Versus-Rebalancing

Impermanent Loss (IL) traditionally served as the primary risk metric for LPs. However, IL conflates directional market risk with execution costs; because it is path-independent, it fails to capture the continuous drain of providing liquidity. If an asset's price fluctuates but returns to its initial rate, IL is zero, ignoring the value extracted by arbitrageurs during the volatility. Because CPMMs are passive and rely on stale on-chain pricing, they suffer from information asymmetry against arbitrageurs trading on external markets. Loss-Versus-Rebalancing (LVR) quantifies this adverse selection cost [12]. LVR compares the LP's position to a reference portfolio holding identical asset weights, which rebalances via an external, frictionless market at the marginal price, rather than against arbitrage flow at stale algorithmic quotes.

To formalize this penalty, AMM dynamics are analyzed within a continuous-time Black-Scholes framework [4]. The LP's position is equivalent to a short position in exotic options, where LVR acts as the funding fee paid to arbitrageurs [12]. Over a time horizon t , accumulated LVR is the path-dependent integral of instantaneous price variance multiplied by the marginal pool value:

$$\text{LVR}_t = \int_0^t \frac{\sigma_s^2}{8} V(P_s) ds \quad (1)$$

This equation dictates that LVR relies on the instantaneous stochastic volatility trajectory (σ_s) and the physical capital exposed to the marginal price path $(V(P_s))$. Consequently, in standard CPMMs where 100% of capital must be exposed to maintain depth, higher market turbulence guarantees a continuous drain on LP profitability.

3 Related Work

In this section, we categorize previous works into three primary domains: first, the formalization of LVR as the definitive metric for adverse selection; second, the development of incentive-compatible mechanism designs and their inherent trade-offs with market efficiency; and finally, structural and derivative-hybrid models that attempt to internalize risk through off-chain auctions or asymmetric pricing functions. By analyzing the limitations of these existing frameworks, we highlight the unique research gap that an endogenous structural approach must address.

3.1 Formalizing Adverse Selection: The LVR Framework

The emergence of LVR as a risk metric has redefined the understanding of LP profitability. [12] provided the foundational definition of LVR, establishing it as the opportunity cost

of providing liquidity against informed arbitrageurs compared to a frictionless rebalancing portfolio. This framework mathematically proves that LVR is path-dependent and grows with realized volatility ($\frac{\sigma^2}{8}$), a structural drain that IL fails to capture.

Building upon this foundation, [15] further formalized the temporal nature of this loss by modeling AMM positions as continuous-installment options. By characterizing LVR as a continuous “funding fee” paid by LPs to maintain their short-volatility exposure, their work bridges AMM dynamics with classical derivative pricing, specifically equating LVR to the continuous theta decay of the LP’s position. Beyond theoretical modeling, the empirical impact of LVR was solidified by recent studies demonstrating that CEX-DEX arbitrage constitutes the vast majority of extracted MEV on Ethereum, compounding the foundational MEV challenges first identified in classic literature [1, 8]. Together, these works establish that LVR is not merely an abstract cost but a deterministic depletion of capital driven by information asymmetry, execution latency, and the inherent optionality of the AMM pricing curve.

3.2 Mechanism-Level Mitigation and the Incentive Compatibility Trilemma

While concentrated liquidity models [2] vastly improved capital efficiency, they inherently amplified LP exposure to toxic flow, causing recent literature to pivot toward mechanism design as a primary defense against LVR. [6] proposed an incentive-compatible (IC) AMM mechanism that utilizes batched transactions and pre-defined sequencing rules to ensure that a user’s dominant strategy is to report their true valuation, thereby stripping miners of risk-free arbitrage profits. However, as formalized in the AMM Mechanism Design Trilemma, this strong notion of IC inherently precludes market efficiency. Specifically, the batching mechanisms required for IC often ignore orders that fall outside the initial pool price, leading to unfulfilled demand even when trade execution is mathematically feasible.

Consequently, existing mechanism designs force a binary choice: either enforce strict IC at the cost of local market efficiency, or allow efficiency while remaining vulnerable to strategic manipulation. A structural approach that preserves execution efficiency without requiring restrictive batching or sequencing rules remains a critical open challenge.

3.3 Structural and Derivative-Hybrid Mitigations

In response to the LVR challenge, several architectures have attempted to modify the AMM’s core invariant or execution logic. CoW Swap [7] introduces an off-chain batch auction mechanism that matches orders internally, effectively neutralizing continuous LVR by clearing trades at a uniform price. However, this relies on third-party solvers and sacrifices synchronous on-chain composability. Alternatively, hybrid models attempt to internalize risk through derivative-like structures. GammaSwap [9] treats the liquidity position as a short volatility play, allowing users to trade against IL as if it were an option, though it remains reactive and oracle-dependent. Similarly, pvpAMM [14] introduces an asymmetric pricing function to resolve the internal imbalance between long and short positions in perpetual markets. While pvpAMM optimizes for the internal equilibrium of speculative players, it does not address the external imbalance, the LVR-driven drain caused by the discrepancy between the AMM and highly liquid external markets.

Crucially, these models generally assume routine market conditions and lack an endogenous mechanism to guarantee micro-resilience against sudden liquidity crunches. They often either move execution off-chain or introduce complex, high-latency derivative layers. Thus, there is

a distinct need for an endogenous structural defense that proportionally reduces LVR while preserving the atomic nature of spot AMMs and ensuring resilience against acute volatility spikes.

4 The HLCP Architecture: Re-engineering Passive Liquidity

In automated market making, protocols face a fundamental geometric trap: attempting to minimize execution slippage for retail users by expanding pool depth mechanically amplifies the LVR exposure for LPs. Traditional CPMMs treat a trade as a single monolithic event on a curve. However, this perspective overlooks a critical geometric dichotomy: a single swap generates both a secant line (representing the trader's actual execution cost) and a new tangent line (representing the pool's shifted marginal price, which arbitrageurs immediately exploit). The systemic inefficiencies of modern AMMs stem directly from the attempt to force these two geometric lines into convergence using a single, static pool of capital.

In this section, we recast the CPMM problem in geometric terms and introduce the Hybrid Liquidity-Collateral Pool (HLCP) as a stylized alternative to uniform full-reserve scaling. The aim is not to claim exact secant-tangent convergence under finite capital, but to study whether separating execution depth from continuously exposed capital can improve the trade-off faced by LPs. We proceed in three steps:

1. **The Geometric Limits of Passive Liquidity (Section 4.1):** We formalize the divergence between execution slippage (S) and marginal-price deviation (Δp), and identify a saturation region in which additional physical liquidity yields limited execution improvement while maintaining exposure to toxic arbitrage.
2. **The N -Scaling Architecture and Kinetic Trigger (Section 4.2):** We present the HLCP decomposition into active reserves and a collateral buffer, and define a trigger-based collateral injection rule that expands active depth along a price-ratio-preserving direction when marginal-price deviations become economically meaningful.
3. **Protocol Economics and Dynamic Execution Equivalence (Section 4.3):** We study a tolerance-bounded execution argument together with a stylized duopoly game. Under the stated saturation, routing, volatility, and collateral-yield assumptions, the HLCP action emerges as a Nash equilibrium of that model.

4.1 Limits of Passive Liquidity and Marginal Price Dynamics

While CPMMs offer a robust mechanism for on-chain price discovery, the relationship between liquidity depth (L) and execution quality is inherently non-linear. As L surpasses a critical saturation threshold, the marginal utility of further capital injection for reducing slippage approaches an asymptotic limit. Beyond this point, excess passive liquidity contributes negligibly to trade execution while exponentially increasing the pool's exposure to toxic arbitrage (i.e., LVR). This subsection models the diminishing returns of slippage reduction to establish the structural necessity for capital decoupling. By defining the explicit geometric divergence between execution slippage and marginal price deviation, we provide the strict mathematical prerequisite for the Kinetic Trigger mechanism introduced in subsequent sections.

Consistent with the constant product invariant $x \cdot y = L^2$, we define L as the pool's liquidity depth. To rigorously quantify the structural inefficiencies of passive capital, it is essential to mathematically separate the theoretical marginal price from the effective execution price obtained during a discrete trade.

► **Definition 1** (Marginal and Effective Price). *Let x and y denote the pool reserve balances. The marginal price P represents the tangent line to the CPMM curve at the current state, defined as $P = \frac{y}{x}$. For a discrete trade volume Δx , the effective price P_{eff} represents the secant line intersecting the pre-trade and post-trade states, defined as:*

$$P_{eff} = \frac{\Delta y}{\Delta x} \quad (2)$$

Consequently, the absolute geometric divergence between the tangent line and the secant line directly quantifies the execution slippage (S). Mathematically, this slippage is the strictly positive penalty imposed by the curve’s convexity, expressed as $S \propto |P - P_{eff}|$.

► **Lemma 2** (Asymptotic Convergence of Effective Price). *For any trade size $\Delta x > 0$, the effective price P_{eff} (secant line) asymptotically converges to the marginal price P (tangent line) as the pool liquidity L approaches infinity.*

Proof. Based on Definition 1 and the invariant $x \cdot y = L^2$, the asset balances are parameterized as $x = L/\sqrt{P}$ and $y = L\sqrt{P}$. When a trade Δx is executed, the pool state shifts such that $(x + \Delta x)(y - \Delta y) = L^2$. Isolating the output yields $\Delta y = y - \frac{L^2}{x + \Delta x}$. By substituting these parameterized expressions, we derive the effective price P_{eff} and take its limit as liquidity approaches infinity:

$$P_{eff} = \frac{P}{1 + \frac{\Delta x \sqrt{P}}{L}} \implies \lim_{L \rightarrow \infty} P_{eff} = P \quad (3)$$

This mathematically confirms that the secant line representing the effective price aligns perfectly with the tangent line of the marginal price under infinite liquidity, thereby nullifying the geometric price impact. ◀

► **Definition 3** (Slippage). *Building upon this geometric divergence, let the slippage S be formally defined as the relative price impact incurred by a trade of size Δx . It is computed by normalizing the absolute deviation of the effective execution price P_{eff} against the theoretical marginal price P . By algebraically substituting the price ratio P_{eff}/P derived in (3) and expressing it in terms of the pre-trade balance x , we obtain:*

$$S(L) = \frac{P - P_{eff}}{P} = 1 - \frac{P_{eff}}{P} = 1 - \frac{x}{x + \Delta x} = \frac{\Delta x}{x + \Delta x} \quad (4)$$

► **Lemma 4** (Convexity and Diminishing Returns of Liquidity). *For a fixed trade size $\Delta x > 0$ and marginal price P , the slippage function $S(L)$ is strictly convex with respect to the liquidity depth L . This establishes that the marginal utility of expanding physical liquidity strictly diminishes and approaches zero asymptotically.*

Proof. Based on the CPMM $x = \frac{L}{\sqrt{P}}$, let $K = \Delta x \sqrt{P}$ represent a strictly positive, trade-specific constant. Substituting x into Definition 3 yields the generalized slippage function and its derivatives:

$$S(L) = \frac{K}{L + K}, \quad \frac{dS}{dL} = -\frac{K}{(L + K)^2} < 0, \quad \frac{d^2S}{dL^2} = \frac{2K}{(L + K)^3} > 0$$

Because $K, L > 0$, the function is trivially decreasing and strictly convex. This property mathematically enforces the law of diminishing returns: the marginal reduction in slippage obtained per unit of added capital decays quadratically, $\propto 1/(L + K)^2$, with respect to liquidity depth. Thus, beyond a specific saturation point, deploying additional physical capital yields negligible execution improvements. ◀

To quantify this state of capital inefficiency, we formally define the practical saturation threshold (L_{sat}) as the liquidity depth at which the marginal reduction in slippage falls below a negligible constant ϵ . Mathematically, this boundary is established when $\left| \frac{dS}{dL} \right| \leq \epsilon$:

$$\frac{K}{(L+K)^2} \leq \epsilon \implies L_{sat} \geq \sqrt{\frac{K}{\epsilon}} - K$$

In practice, the theoretical threshold ϵ is not an arbitrary constant, but is structurally dictated by the market microstructure of external venues. Specifically, ϵ represents the fundamental frictional bounds of CEXs, comprising the minimum tick size and baseline trading fees (e.g., 1-5 bps). If the marginal reduction in DEX slippage falls below this exogenous tick resolution, the price improvement becomes economically invisible to both retail traders and arbitrageurs. Consequently, for major pairs like ETH/USDC, standard order flow (K) reaches this frictional saturation point ($\approx \epsilon$) long before utilizing the pool's full depth. Any physical liquidity strictly greater than this threshold ($L > L_{sat}$) is mathematically and economically "lazy." It provides negligible additional execution benefit at the chosen (ϵ)-threshold in trade execution while continuously subjecting LPs to uncompensated, structural LVR exposure.

Until now, our analysis has focused on the execution slippage $S(L)$, the geometric penalty (secant line) experienced by an honest retail trader. However, toxic arbitrageurs extracting LVR do not interact with the secant line; they attack the pool's post-trade marginal price (tangent line). To mathematically prove why simply increasing passive liquidity fails to neutralize LVR, we must define the geometric divergence between the trader's execution price and the arbitrageur's target price.

► **Definition 5 (Marginal Price Deviation).** *While the slippage $S(L)$ bounds the secant line from the trader's perspective, the marginal price deviation Δp measures the absolute state shift of the tangent line from the pool's perspective. It is defined as the relative difference between the initial spot price P_0 and the new marginal spot price P_{new} at the exact moment the swap concludes:*

$$\Delta p = \frac{P_0 - P_{new}}{P_0} \quad (5)$$

► **Lemma 6 (Divergence of Execution and Market Pricing).** *For any positive trade volume $\Delta x > 0$, the marginal price deviation strictly exceeds the execution slippage ($\Delta p > S(L)$). This geometric divergence demonstrates that stabilizing $S(L)$ at L_{sat} is entirely insufficient to neutralize LVR exposure.*

Proof. Let $K = \Delta x \sqrt{P_0}$. The execution slippage is established as $S(L) = \frac{K}{L+K}$. Upon executing the trade, the new reserve balances become $x_{new} = x + \Delta x$ and, based on the invariant, $y_{new} = \frac{L^2}{x+\Delta x}$. The new marginal price is trivially the ratio of these new reserves ($P_{new} = \frac{y_{new}}{x_{new}}$), which simplifies to $P_{new} = \frac{L^2}{(x+\Delta x)^2}$. By substituting $x = \frac{L}{\sqrt{P_0}}$, the price deviation computes to:

$$\Delta p = 1 - \frac{P_{new}}{P_0} = 1 - \frac{L^2}{(L + \Delta x \sqrt{P_0})^2} = \frac{(L+K)^2 - L^2}{(L+K)^2} = \frac{2LK + K^2}{(L+K)^2} \quad (6)$$

By factoring this relation against $S(L)$, we derive an exact quadratic correspondence:

$$\Delta p = \left(\frac{K}{L+K} \right) \times \left(\frac{2L+K}{L+K} \right) = S(L) \cdot (2 - S(L)) \quad (7)$$

Since $S(L) > 0$ for any non-zero trade, it strictly follows that $(2 - S(L)) > 1$. Therefore, $\Delta p > S(L)$ always holds true. Specifically, for standard retail trades where $S(L)$ is small and

approaches 0, the marginal price deviation approaches exactly twice the magnitude of the execution slippage: $\Delta p \approx 2S(L)$ ◀

► **Example 7 (The $2\times$ Arbitrage Exploit).** To illustrate the economic severity of this geometric divergence, consider an external market shock where the true price of an asset on a CEX increases by 2%. To extract maximum risk-free profit, an arbitrageur must push the DEX’s marginal price to match the CEX, targeting a marginal price deviation of $\Delta p = 2\%$. However, strictly governed by the $\Delta p \approx 2S(L)$ multiplier, the arbitrageur incurs an execution slippage of only $S(L) \approx 1\%$ to move the tangent line by 2%. Consequently, the arbitrageur buys the underpriced asset on the DEX at a 1% geometric penalty (secant cost) and immediately liquidates it on the CEX at a 2% premium (tangent target), deterministically pocketing a 1% risk-free margin (LVR) at the direct expense of LPs.

► **Remark 8 (The Core Dilemma and Architectural Prerequisite).** This structural exploit mathematically proves why passive liquidity scaling is a definitive failure to neutralize LVR. If a protocol attempts to defend against this exploit by injecting massive physical liquidity ($L \rightarrow \infty$) to suppress the execution slippage $S(L)$ down to 0.01%, the marginal price deviation Δp inherently shrinks to 0.02%. The 1 : 2 ratio remains immutable. The arbitrageur will simply pay 0.01% in slippage to extract a 0.02% price discrepancy, continually draining the pool. Because this vulnerability is hardcoded into the curve’s convexity, attempting to protect the pool by holding $L > L_{sat}$ is structurally futile. Therefore, to effectively intercept LVR, the protocol must abandon passive scaling. It requires a bifurcated architecture that defends the tangent line (Δp) entirely independently of the secant line ($S(L)$). This necessitates the N -scaled Hybrid Liquidity-Collateral Pool (HLCP) introduced in the following sections.

4.2 The Hybrid Pool Architecture: Inner-Product State Binding

In this section, we formalize the Hybrid Liquidity-Collateral Pool (HLCP), an architecture designed to functionally decouple capital provision from market-making exposure. While Section 4.1 demonstrated that marginal utility diminishes as liquidity saturates, the HLCP internalizes this “laziness” by bifurcating the liquidity vector into an active capacity for the constant-product curve and a low-risk yield collateral buffer.

4.2.1 The N -Scaling Mechanism and Virtual Invariant

The primary mechanism of the HLCP is the N -Scaling of active reserves to maintain price impact parity with a much deeper pool. Let the physical reserves in the active pool be x_a and y_a . To provide an effective depth of L_{total} while utilizing only a fraction of the capital, the AMM operates on a virtual constant-product curve:

$$\left(\frac{x_a}{N}\right) \cdot \left(\frac{y_a}{N}\right) = L_{total}^2 \quad (8)$$

where $N \in (0, 1]$ represents the capital exposure ratio. By setting $N < 1$, the system deploys $L_{active} = N \cdot L_{total}$ into the active market-making capacity, while diverting the residual $C = (1 - N) \cdot L_{total}$ into the collateral buffer.

4.2.1.1 Physical and claimed slippage

Fix a trade size $\Delta x > 0$ and marginal price P , and recall $K = \Delta x \sqrt{P}$ from Lemma 4. We distinguish between the benchmark slippage of the full-depth reference pool and the realized

slippage of the physically active pool:

$$S_{\text{claimed}} := S(L_{\text{total}}) = \frac{K}{L_{\text{total}} + K}, \quad S_{\text{physical}} := S(L_{\text{active}}) = S(NL_{\text{total}}) = \frac{K}{NL_{\text{total}} + K}$$

Because $N \leq 1$, one has $S_{\text{physical}} \geq S_{\text{claimed}}$, with equality only in the limiting cases $N = 1$ or $L_{\text{total}} \rightarrow \infty$. Their exact gap is

$$\Delta S := S_{\text{physical}} - S_{\text{claimed}} = \frac{K(1-N)L_{\text{total}}}{(NL_{\text{total}} + K)(L_{\text{total}} + K)} > 0 \quad (9)$$

Thus the HLCP does *not* claim literal equality between the physical N -scaled curve and the full-reserve benchmark. Instead, for a router tolerance parameter $\varepsilon_{\text{router}} > 0$, we say that the protocol attains *router-acceptance equivalence* at trade size Δx whenever

$$\Delta S \leq \varepsilon_{\text{router}}. \quad (10)$$

Since $(NL_{\text{total}} + K)(L_{\text{total}} + K) \geq NL_{\text{total}}^2$, a sufficient condition for (10) is

$$L_{\text{total}} \geq \frac{K(1-N)}{N\varepsilon_{\text{router}}}. \quad (11)$$

Hence, in hyper-saturated markets, the physical slippage gap can be made arbitrarily small at the router tolerance scale, even though it is never exactly zero for finite L_{total} .

4.2.1.2 Execution objects used below

To avoid ontological ambiguity, we explicitly distinguish three objects throughout the sequel: (i) the executable active depth $L_{\text{active}} = NL_{\text{total}}$, on which swaps are physically settled before trigger activation; (ii) the benchmark depth L_{total} , used only as a reference target for slippage comparison; and (iii) the post-trigger executable depth $L_{\text{new}} = L_{\text{active}} + \Delta C$, on which swaps are physically settled after collateral deployment.

4.2.2 Deterministic Binding via State Vector

Let L_{active} be the baseline liquidity invariant of the active curve ($L_{\text{active}} = \sqrt{x_a \cdot y_a}$), and C be the liquidity-equivalent capacity of the isolated collateral buffer mapped to the invariant space ($L = \sqrt{x \cdot y}$). We define the pool's state allocation vector $\mathbf{\Lambda}$, which partitions the liquidity capacities:

$$\mathbf{\Lambda} = \begin{bmatrix} L_{\text{active}} \\ C \end{bmatrix} \quad (12)$$

The dynamic equilibrium of this allocation is governed by a weight vector $\mathbf{W}(\Delta p)$, which continuously monitors the pool's marginal price deviation, defined as Δp . We formalize this functional binding as:

$$\mathbf{W}(\Delta p) = \begin{bmatrix} \frac{1}{N} \\ \alpha \cdot \phi(\Delta p) \end{bmatrix} \quad (13)$$

The first component, the Leverage Factor ($\frac{1}{N}$), scales the active reserves to establish the virtual invariant's baseline, providing a standardized geometric reference for the kinetic trigger. The second component, the kinetic trigger ($\alpha \cdot \phi(\Delta p)$), dictates the dynamic collateral injection rate. Here, $\alpha > 0$ serves as a strictly positive sensitivity multiplier

governing the aggressiveness of the collateral response, and $\phi : \mathbb{R} \rightarrow \mathbb{R}_{\geq 0}$ is the deterministic activation function $\phi(z) := \max\{0, |z| - \tau\}$ anchored to a baseline tolerance τ , bounded by the pool's base swap fee (f). Because arbitrageur profitability (LVR) is determined by the post-trade marginal price rather than the execution price, Δp must serve as the sole algorithmic sensor. Since micro-deviations ($|\Delta p| \leq f$) render arbitrage unprofitable due to fee friction, the Kinetic Trigger is explicitly designed to remain dormant against benign noise and activate only when the price deviation presents a viable LVR opportunity ($\tau \geq f$).

The deterministic binding between the active capacity and the collateral buffer is strictly governed by the inner product of the weight and state allocation vectors:

$$\langle \mathbf{W}(\Delta p), \mathbf{\Lambda} \rangle = \left(\frac{1}{N} \cdot L_{active} \right) + \left(\alpha \cdot \phi(\Delta p) \cdot C \right) = L_{eff}(\Delta p) \quad (14)$$

When the deviation exceeds the tolerance threshold ($|\Delta p| > \tau$), the kinetic trigger activates. Geometrically, the protocol injects collateral in the spot ratio associated with P_{new} , so the operating point moves along the corresponding price ray. This preserves the instantaneous reserve ratio at the moment of activation while increasing executable depth from L_{active} to $L_{new} = L_{active} + \Delta C$.

Economically, the relevant claim is comparative rather than absolute. The post-trigger curve is physically deeper and locally flatter than the pre-trigger active curve, which reduces the incremental adverse-selection cost of subsequent marginal flow. This does not imply literal identity between the physical post-trigger curve and a benchmark full-depth curve. Rather, under the tolerance-bounded routing condition developed in Section 4.3, it provides an operational approximation that can remain competitively executable in saturated markets.

4.2.3 Dynamic Injection Scalar and Asymptotic Buffer Defense

If a large adverse order moves the pool price, the protocol may shift physical capital ΔC from the collateral buffer into the active pool. The virtual accounting target L_{eff} may exceed the original benchmark depth, but the physically executable post-trigger depth remains $L_{new} = L_{active} + \Delta C \leq L_{total}$.

► **Lemma 9** (Dynamic Injection Scalar). *Under the protocol-enforced control policy below, the trigger-induced collateral deployment ΔC is a bounded rational function of the shock variable $\phi(\Delta p)$. In particular, for every finite shock, the policy implies $\Delta C < C$, so one trigger response cannot exhaust the entire buffer in a single step.*

Proof. Let the post-trigger state vector be $\mathbf{\Lambda}' = [L_{active} + \Delta C, C - \Delta C]^\top$. The post-trigger accounting target is still evaluated through the same weight vector:

$$\langle \mathbf{W}(\Delta p), \mathbf{\Lambda}' \rangle = \frac{1}{N} (L_{active} + \Delta C) + \alpha \cdot \phi(\Delta p) \cdot (C - \Delta C) = L'_{eff}(\Delta p). \quad (15)$$

To impose a one-step bound on deployment, the protocol adopts the control rule

$$\frac{\Delta C}{N} = \alpha \cdot \phi(\Delta p) \cdot (C - \Delta C). \quad (16)$$

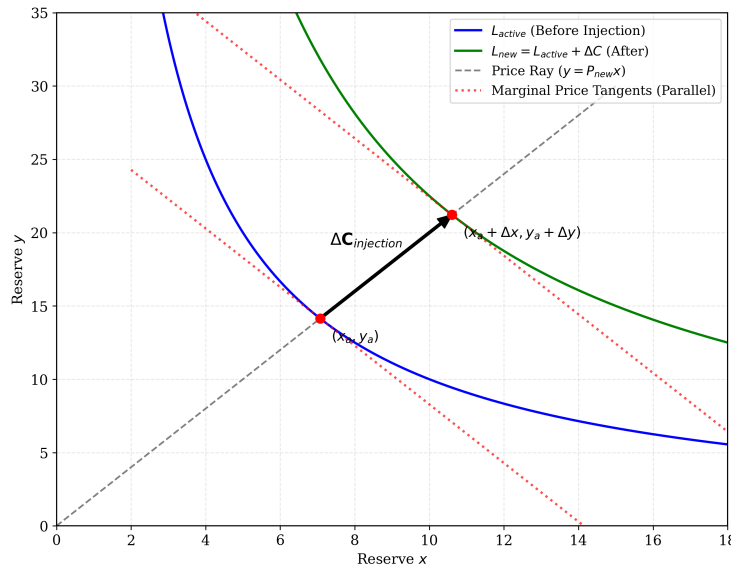
Solving for ΔC yields $\Delta C = \frac{N \cdot \alpha \cdot \phi(\Delta p) \cdot C}{1 + N \cdot \alpha \cdot \phi(\Delta p)}$. For every finite $\phi(\Delta p)$, the denominator strictly exceeds the numerator multiplier, and therefore $\Delta C < C$. The asymptotic envelope is

$$\lim_{\phi \rightarrow \infty} \Delta C = \lim_{\phi \rightarrow \infty} C \left(\frac{N \alpha \phi(\Delta p)}{1 + N \alpha \phi(\Delta p)} \right) = C$$

Thus, the limit describes only the envelope of the policy as the shock grows without bound. Under the chosen control rule, a single trigger response remains bounded away from total depletion for every finite shock. This is a statement about the one-step policy response, not a claim of perpetual solvency under arbitrarily repeated shocks. ◀

4.2.4 The Vectorized Homothety Projection and Price-Neutrality

Crucially, injecting this geometric scalar ΔC must act not as a trade, but as a structural expansion of the curve. Fig. 1 illustrates this vectorized injection process, where the curve expands outward without altering the marginal price.



■ **Figure 1** Schematic illustration of the vectorized homothety projection. The injection vector $\Delta C_{injection}$ scales the active liquidity ($L_{active} \rightarrow L_{new}$) along the price ray, preserving the marginal tangent slope.

► **Lemma 10** (Homothety Projection). *Injecting the vector $\Delta C_{injection} = \frac{\Delta C}{\sqrt{P_{new}}} [1 \ P_{new}]^T$ acts exclusively as a uniform homothety, expanding the absolute liquidity depth by exactly ΔC while strictly preserving the skewed marginal price P_{new} .*

Proof. Given the invariant $L = \sqrt{x \cdot y}$, the geometric expansion of the curve is defined as $\Delta L = \sqrt{\Delta x \cdot \Delta y} = \Delta C$. To inject assets along the constant-price ray, the ratio of the injected reserves must exactly match the current marginal price. Thus, we enforce $\frac{\Delta y}{\Delta x} = P_{new}$, which derives $\Delta x = \frac{\Delta C}{\sqrt{P_{new}}}$ and $\Delta y = \Delta C \sqrt{P_{new}}$. The requisite injection vector, visualized as the outward translation in Fig. 1, is formalized as:

$$\Delta C_{injection} = \frac{\Delta C}{\sqrt{P_{new}}} \cdot \begin{bmatrix} 1 \\ P_{new} \end{bmatrix} = \begin{bmatrix} \Delta x \\ \Delta y \end{bmatrix} \quad (17)$$

Let the pre-injection reserves be (x_a, y_a) such that the marginal price is $P_{new} = \frac{y_a}{x_a}$. By injecting these assets, the new tangent price P' becomes:

$$P' = \frac{y_a + \Delta y}{x_a + \Delta x} = \frac{P_{new}x_a + \Delta C\sqrt{P_{new}}}{x_a + \frac{\Delta C}{\sqrt{P_{new}}}} = \frac{P_{new} \left(x_a + \frac{\Delta C}{\sqrt{P_{new}}} \right)}{x_a + \frac{\Delta C}{\sqrt{P_{new}}}} = P_{new} \quad (18)$$

As depicted in the parallel marginal tangents of Fig. 1, the tangent slope is perfectly preserved during this expansion. Next, we verify the absolute liquidity depth expansion (L_{new}):

$$\begin{aligned} L_{new} &= \sqrt{(x_a + \Delta x)(y_a + \Delta y)} = \sqrt{\left(x_a + \frac{\Delta C}{\sqrt{P_{new}}}\right) \left(P_{new}x_a + \Delta C\sqrt{P_{new}}\right)} \\ &= \sqrt{P_{new} \left(x_a + \frac{\Delta C}{\sqrt{P_{new}}}\right)^2} = x_a\sqrt{P_{new}} + \Delta C \end{aligned}$$

Since the active liquidity is $L_{active} = \sqrt{x_a \cdot y_a} = x_a\sqrt{P_{new}}$, it follows that $L_{new} = L_{active} + \Delta C$.

This geometric proof shows that the operating point moves along the price ray without changing the instantaneous reserve ratio. Accordingly, the trigger step does not itself introduce an additional reserve-ratio discontinuity that would create a separate backrunning opportunity at the instant of activation. ◀

4.3 Protocol Economics and Capital Efficiency

Having formalized the geometric mechanisms of the kinetic trigger in the preceding subsection, we now study their economic implications in a stylized setting. The purpose of this subsection is limited. First, we state a tolerance-bounded execution argument for saturated markets, clarifying when reduced active capital may remain competitively executable. Second, we analyze a stylized duopoly game to examine whether, under the stated liquidity-saturation, routing, volatility, and collateral-yield assumptions, the HLCP action can outperform the standard-AMM action.

4.3.1 Tolerance-Bounded Execution and Slippage Defense

A critical critique of any capital segregation model is the intuitive assumption that reducing active liquidity ($N < 1$) necessarily degrades execution quality and repels fee-generating volume. The HLCP does not answer this critique by asserting literal equality between the active N -scaled curve and a fully funded CPMM. Rather, it answers it in two steps. First, for routine order sizes in saturated markets, the slippage gap $\Delta S := S_{physical} - S_{claimed}$ can fall below a router tolerance threshold ε_{router} , as characterized in (10). Second, when the deviation becomes economically material, the kinetic trigger deploys collateral so that execution continues on a physically flatter post-trigger curve.

This tolerance-bounded defense can be summarized in three operational facts. First, under proportional N -scaling, the instantaneous marginal price is unchanged, $P' = \frac{N \cdot y}{N \cdot x} = \frac{y}{x} = P$, so moving from full reserves to active reserves does not by itself distort the local tangent price. Second, for routine trade sizes, the relevant execution claim is the bounded condition (10): $S_{claimed}$ is a benchmark quotation target, while settlement remains on the physical active curve. Third, if the deviation becomes economically material, the kinetic trigger injects collateral from the dormant buffer so that execution proceeds against the enlarged post-trigger depth $L_{new} = L_{active} + \Delta C$ rather than against the original N -scaled reserve alone.

While the active engine handles the swap logic, the sequestered collateral buffer (C) is assumed to earn an exogenous baseline yield by being deposited into standard, risk-isolated ERC-4626 vaults [13]. This auxiliary yield is represented by Y_C in the stylized payoff model below; it is not needed for the geometric analysis above, but it provides an additional channel through which lower active exposure may affect LP outcomes.

4.3.2 Game Theoretical Analysis: Liquidity Saturation and Nash Equilibrium

We model these incentives through a saturated-market duopoly with large background liquidity.

► **Proposition 11** (Yield Dilution under Saturated Liquidity). *Let F denote the aggregate daily swap fee revenue generated by the AMM, where each LP extracts a fractional yield $f = \frac{F}{L_{total}}$ proportional to their liquidity share. The marginal utility of adding liquidity to the pool is strictly piecewise, governed by a saturation threshold L_{sat} .*

Economically, this saturation threshold dictates that when $L_{total} < L_{sat}$, additional liquidity can still reduce execution frictions and may therefore support higher aggregate fee revenue F . Once $L_{total} > L_{sat}$ for the trade sizes under consideration, further liquidity has limited marginal effect on slippage, so fee revenue is reasonably modeled as approaching an upper bound F_{max} . In that regime, the per-unit fee yield $f = \frac{F_{max}}{L_{total}}$ declines as total active liquidity expands, while LVR continues to scale with active exposure. This observation motivates, rather than by itself proves, the stylized payoff comparison below.

4.3.2.1 The Duopoly Game Formulation

To study that comparison, we model a highly saturated market using a two-player game augmented with large exogenous background liquidity.

► **Remark 12** (Assumption on Proportional Fee Routing). While real-world order routing by DEX aggregators involves highly complex endogenous dynamics, this stylized duopoly game assumes proportional fee routing. Specifically, invoking the tolerance-bounded routing condition $\Delta S \leq \varepsilon_{router}$ from Section 4.2, we assume that, for standard retail trades in saturated markets, this bound is sufficient for routers to treat the HLCP as competitively executable. This is a stylized assumption about router acceptance, not a claim that the physical and benchmark curves are identical.

We evaluate all strategic payoffs over a unified time horizon $T > 0$, measured in years. Let $F_{max}(T)$ denote the aggregate fee revenue earned by the saturated meta-market over this horizon. Under the constant-volatility approximation used below, define the cumulative LVR of active capital W over T by

$$\text{LVR}_W(T) := \frac{\sigma^2}{8}WT, \quad (19)$$

which is the constant- $V(P_t) = W$ specialization of (1). Let r_c denote the annualized collateral yield rate on dormant capital, and define the corresponding cumulative collateral yield over horizon T by $Y_C(T) := (1 - N)Wr_cT$. All payoff entries below are therefore expressed in currency units over the same horizon T ; no term mixes daily, instantaneous, and annualized quantities.

Let X denote the massive, pre-existing passive liquidity in the broader market pair ($X \gg L_{sat}$). Assuming trade volume is routed strictly proportionally to active market depth, a player's fee payoff over horizon T is determined by its fraction of total active liquidity (including X), multiplied by $F_{max}(T)$. The adverse selection cost scales with active exposure through $\text{LVR}_W(T)$, and the dormant buffer earns $Y_C(T)$.

$$\begin{aligned}\pi_{std,std}(T) &= \left(\frac{W}{X + 2W} \right) F_{\max}(T) - \text{LVR}_W(T), \\ \pi_{HLCP,std}(T) &= \left(\frac{N \cdot W}{X + (1 + N)W} \right) F_{\max}(T) - N \cdot \text{LVR}_W(T) + Y_C(T), \\ \pi_{std,HLCP}(T) &= \left(\frac{W}{X + (1 + N)W} \right) F_{\max}(T) - \text{LVR}_W(T), \\ \pi_{HLCP,HLCP}(T) &= \left(\frac{N \cdot W}{X + 2N \cdot W} \right) F_{\max}(T) - N \cdot \text{LVR}_W(T) + Y_C(T).\end{aligned}$$

Player A \ Player B	Std AMM (W active)	HLCP ($N \cdot W$ active)
Std AMM (W active)	$(\pi_{std,std}, \pi_{std,std})$	$(\pi_{std,HLCP}, \pi_{HLCP,std})$
HLCP ($N \cdot W$ active)	$(\pi_{HLCP,std}, \pi_{std,HLCP})$	$(\pi_{HLCP,HLCP}, \pi_{HLCP,HLCP})$

■ **Table 1** Strategic Payoff Matrix under Liquidity Saturation

► **Theorem 13** (Nash Equilibrium under Hyper-Saturation). *Under hyper-saturated background liquidity ($X \rightarrow \infty$), and provided that local market volatility is strictly positive ($\sigma > 0$) or the collateral yield rate is non-zero ($r_c > 0$), the HLCP action yields a strictly higher payoff than the standard-AMM action in the stylized two-player game above. Hence the (HLCP, HLCP) profile is the unique Nash equilibrium of that limit game.*

Proof. To establish this strict dominance beyond algebraic limits, we evaluate the unilateral deviations through an economic lens. Under hyper-saturation, the aggregate fee revenue asymptotically plateaus at a maximum bound F_{max} .

Step 1: Unilateral Deviation (Scenario A). Consider the case where Player B commits to the Standard AMM. For Player A to deviate to the HLCP, the condition $\pi_{HLCP,std} > \pi_{std,std}$ must hold. To operationalize this condition within a static snapshot, we transition from the cumulative LVR integral to an instantaneous expected rate via its time derivative. Under the unit convention above, the cumulative LVR over horizon T is $\text{LVR}_W(T) = \frac{\sigma^2}{8}WT$. By substituting this instantaneous rate and rearranging the payoff functions, the deviation inequality reduces to comparing the defensive yield gains against the fee opportunity cost (ΔF):

$$(1 - N)W \left(\frac{\sigma^2}{8} + r_c \right) T > \Delta F(T), \quad (20)$$

where $\Delta F(T) := F_{\max}(T) \cdot W \left(\frac{1}{X+2W} - \frac{N}{X+(1+N)W} \right)$. Since $T > 0$ is common to all terms, the inequality is equivalent to $(1 - N) \left(\frac{\sigma^2}{8} + r_c \right) > \frac{\Delta F(T)}{WT}$. As $X \rightarrow \infty$, the fee-loss term vanishes, so the deviation condition collapses to $(1 - N) \left(\frac{\sigma^2}{8} + r_c \right) > 0$.

Step 2: The Free-Rider Vulnerability (Scenario B). Assume Player B attempts to opportunistically defect to the standard CPMM ($N = 1$) while Player A remains committed to the HLCP. For the cooperative HLCP state to be a strictly stable Nash Equilibrium against this free-rider defection, the stability condition $\pi_{HLCP,HLCP} > \pi_{std,HLCP}$ must hold.

By substituting the instantaneous expected rate ($LVR_W = W \frac{\sigma^2}{8}$) and accumulating over horizon T , the inequality simplifies to:

$$(1 - N)W \left(\frac{\sigma^2}{8} + r_c \right) T > \Delta F'(T), \quad (21)$$

where $\Delta F'(T)$ represents the cumulative marginal fee gain captured by the defection. Since $T > 0$ is common to all terms, the stability inequality is equivalent to $(1 - N) \left(\frac{\sigma^2}{8} + r_c \right) > \frac{\Delta F'(T)}{WT}$. As $X \rightarrow \infty$, the hyper-saturated routing benefit vanishes ($\lim_{X \rightarrow \infty} \frac{\Delta F'(T)}{WT} = 0$). Consequently, the stability inequality collapses to the identical conditional state:

$$(1 - N) \left(\frac{\sigma^2}{8} + r_c \right) > 0. \quad (22)$$

Under the theorem assumptions, the HLCP action therefore yields a strictly higher payoff than reverting to the standard-AMM action in this stylized limit game. ◀

► **Corollary 14** (Macro-Equilibrium and Pareto Improvement in the Stylized Limit). *In the symmetric hyper-saturated limit, if background liquidity also compresses active exposure proportionally to N , then the individual fee share is unchanged:*

$$\frac{N \cdot W}{N \cdot X + 2N \cdot W} = \frac{W}{X + 2W}$$

Consequently, in this stylized limit, players preserve the same fee share while reducing active LVR exposure by the factor N and adding collateral yield $Y_C(T)$. Under the maintained assumptions, the HLCP outcome Pareto-improves on the standard-AMM outcome.

5 Empirical Validation and Discussion

This section presents a two-tiered empirical validation of the HLCP architecture. The purpose is not to claim market-complete validation, but to evaluate two bounded questions in sequence. First, **Experiment 1 (Micro-Resilience and Buffer Integrity)** tests whether the trigger rule remains bounded away from one-shot total depletion under an explicitly adversarial stochastic-volatility-with-jumps (SVJ) stress path at 12-second block resolution. Second, **Experiment 2 (Long-term Historical Backtest)** evaluates whether lower active exposure can improve realized net LP outcomes on the 2025 ETH path under the conservative assumption $Y_C(T) = 0$. This ordering separates mechanism stress testing from long-horizon profitability measurement.

5.1 Experiment 1: Structural Resilience under Stochastic Volatility Shocks

Experiment 1 serves as an empirical stress test evaluating the mechanical dynamics of the HLCP during systemic crises. Departing from random walk assumptions, we implement a Stochastic Volatility with Jumps (SVJ) framework governed by a Cox-Ingersoll-Ross (CIR) process. This architecture simulates the high-frequency, non-linear dynamics of DeFi markets, creating a hostile environment to evaluate LVR exposure.

5.1.1 The Coupled Dynamics: From Variance to Price

The stress environment is generated by coupled CIR-SVJ dynamics. The variance process is

$$dV_t = \kappa(\theta - V_t)dt + \xi\sqrt{V_t}dW_t^V \quad (23)$$

It fulfills a critical dual mandate within the simulation. First, its diffusion term ($\xi\sqrt{V_t}dW_t^V$) introduces the stochastic “volatility of volatility,” ensuring that the market’s friction is never static but subject to continuous, unpredictable fluctuations. Second, and more importantly during a crisis, its drift term ($\kappa(\theta - V_t)dt$) acts as a mean-reverting gravitational force that pulls the variance toward a long-term baseline (θ) at a speed of κ . Following a systemic shock where the variance regime shifts ($\theta \rightarrow \theta_{shock}$), this mechanism ensures that the inflated variance eventually decays back to a normal equilibrium, mimicking the market’s natural “cooling off” period.

Building upon this, the price process is modeled as a stochastic-volatility jump diffusion. Let W_t^V and W_t^\perp be independent standard Brownian motions and define

$$dW_t^S := \rho dW_t^V + \sqrt{1 - \rho^2} dW_t^\perp, \quad \rho \in [-1, 1]. \quad (24)$$

Then $d\langle W^S, W^V \rangle_t = \rho dt$, so ρ controls the instantaneous correlation between variance shocks and price shocks. The coupled dynamics are therefore governed by (23) and

$$dS_t = \mu S_{t-} dt + \sqrt{V_t} S_{t-} dW_t^S + S_{t-} dJ_t, \quad dJ_t := (e^{Y_t} - 1) dN_t, \quad (25)$$

where $(N_t)_{t \geq 0}$ is a Poisson process with intensity λ_J , the jump marks Y_t are i.i.d. $\mathcal{N}(\mu_J, \sigma_J^2)$, and S_{t-} denotes the left limit of the price process at jump times. Equivalently, e^{Y_t} is the gross jump multiplier, so $\mu_J < 0$ produces downward jumps on average. It is important to distinguish the roles of the two stochastic mechanisms. The term $\sqrt{V_t} S_{t-} dW_t^S$ captures continuous diffusion under stochastic variance, whereas dJ_t captures discrete price discontinuities.

Time is measured in years, with $\Delta t = \frac{12}{365 \times 24 \times 3600}$. The state variable V_t is annualized variance, so the Euler-step diffusion scale is $\sqrt{V_t} \Delta t$. If σ_{annual} denotes annualized volatility, then the corresponding per-step volatility is $\sigma_{step} = \sigma_{annual} \sqrt{\Delta t}$, while the corresponding baseline variance level is $\theta_{base} = \sigma_{annual}^2$. We calibrate $\sigma_{annual} \approx 74.56\%$ from the realized 2025 ETH path (sourced via Etherscan) used in the backtest.

5.1.2 Adversarial Regime Calibration

The stress scenario contains two distinct shock channels. First, at the designated crisis time t_s , we impose a negative price jump in the SVJ component by conditioning on a jump arrival in the Poisson process N_t and drawing its size from the lognormal jump law in (25); this is the role of dJ_t . Second, independently of the jump term, we shift the variance target in the CIR process from θ_{base} to an elevated crisis regime $\theta_{shock} = 20\theta_{base}$ over the stress window. This separation keeps jump risk strictly in the price equation and variance stress strictly in the variance equation, eliminating the category error between price jumps and variance shocks.

The transmission of this volatility shock into the asset price is governed by an endogenous liquidity crunch mechanism. By introducing a negative correlation ($\rho = -0.5$) between the price diffusion and the variance process, we replicate the mechanics of DeFi liquidation spirals. This architecture serves two structural purposes:

- (a) From (24), the variance of the component of the price diffusion that is correlated with variance shocks is $\rho^2 dt$. With $\rho = -0.5$, one quarter of one-step Brownian variance is carried by the variance-correlated component and three quarters by the orthogonal component. We use this only as a decomposition of the diffusion driver, not as a structural claim about observed market variance shares.
- (b) The negative sign of ρ governs the directional mechanics of the crisis. The linear diffusion equation, (24), demonstrates how shocks are transmitted. When a systemic panic triggers a massive volatility spike ($dW_t^V > 0$), the negative correlation introduces a downward component in the correlated part of the price diffusion ($dW_t^S < 0$).

Together, this mechanism orchestrates the endogenous dynamics where panic triggers a cascading price crash.

To maintain the physical fidelity of this hostile environment, we must prevent the variance from devolving into a predictable deterministic decay. We inject significant stochastic noise (ξ), which is strictly calibrated to satisfy the Feller Condition ($2\kappa\theta_{base} \geq \xi^2$). Utilizing the baseline variance for this calibration ensures that the variance process remains strictly positive and mathematically robust across all regimes, delivering maximum stochastic stress to the kinetic trigger without inducing numerical instability.

5.1.3 Mechanism Dynamics: Active Concentration and Buffer Integrity

For Experiment 1, the trigger sensor is implemented as a stress-diagnostic proxy rather than as a full reserve-path arbitrage simulation. Direct numerical evaluation of (1) in this setting would require an endogenous arbitrage-reserve simulator specifying, at each 12-second step, arbitrageur arrival times, fee-induced no-trade regions, and routing behavior across available liquidity. Because the objective of Experiment 1 is instead to isolate the local responsiveness of the HLCP control rule under a prescribed crisis path, Panel A uses a reduced-form stress proxy that preserves the trigger geometry while abstracting from those additional equilibrium layers.

Let S_t denote the exogenous crisis price path generated by the coupled SVJ process, and define the one-step trigger input by

$$\delta p_t := \left| \frac{S_{t+\Delta t}}{S_t} - 1 \right|, \quad \phi_t := \max\{0, \delta p_t - \tau\}. \quad (26)$$

The standard-AMM path in Panel A is then computed from the stylized capital-loss proxy

$$\ell_{t+\Delta t}^{std} = \ell_t^{std} + K_t^{std} \frac{\phi_t^2}{8}, \quad (27)$$

where K_t^{std} denotes the currently exposed benchmark capital. For the HLCP, the control rule implies

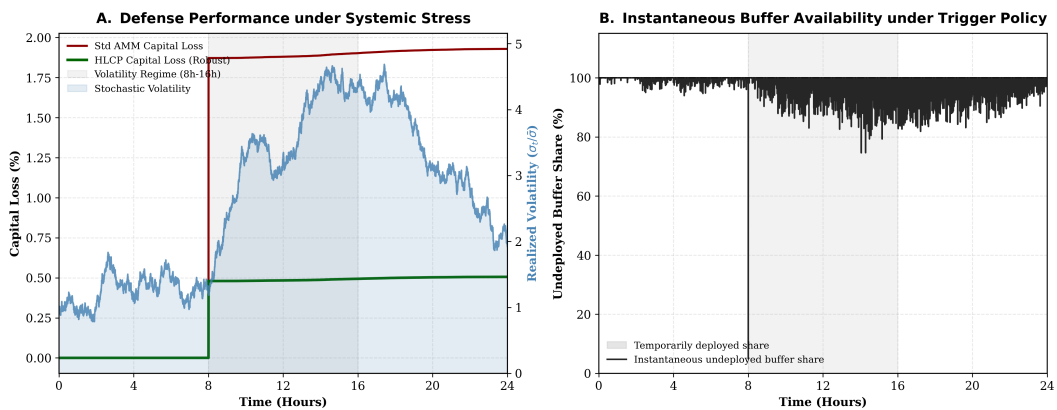
$$\Delta C_t = \frac{N\alpha\phi_t C_t}{1 + N\alpha\phi_t}, \quad K_t^{new} := K_t^{act} + \Delta C_t, \quad (28)$$

and the corresponding stress-path loss proxy is attenuated by the post-trigger depth ratio:

$$\ell_{t+\Delta t}^{HLCP} = \ell_t^{HLCP} + K_t^{act} \frac{\phi_t^2}{8} \cdot \frac{K_t^{act}}{K_t^{new}}. \quad (29)$$

Accordingly, Panel A should be interpreted as a controlled stress-path capital-loss proxy induced by the trigger variable, not as a direct numerical discretization of the continuous-time LVR integral in (1).

Fig. 2 reports the resulting stress-path comparison between the HLCP and a standard CPMM. In Panel A, the forced negative jump at $t = 8$ hours, together with the temporary shift to θ_{shock} , moves the market into the crisis regime. Along this path, the standard AMM accumulates materially larger stress-path capital loss than the HLCP throughout the stress window. By the end of the 8-hour crisis interval ($t = 16$ hours), the standard AMM reaches a cumulative capital loss of approximately 1.90%, whereas the HLCP reaches approximately 0.49%. Over the full 24-hour simulation, the losses settle at 1.93% and 0.51%, respectively, implying an approximately 73.8% lower cumulative loss for the HLCP on this path. The point of the experiment is therefore not that the trigger avoids deployment under stress; it is that, under an explicitly adverse path, the trigger can deploy aggressively enough to cap loss growth while remaining bounded away from one-shot exhaustion under the imposed control rule.



■ **Figure 2** SVJ stress-path comparison between the standard AMM and the HLCP. (A) Cumulative capital-loss trajectories during the forced jump, the elevated-variance window (8–16 hours), and the subsequent relaxation. (B) Instantaneous policy-implied undeployed buffer share under the trigger rule. Immediately after the forced jump, the undeployed share falls to approximately 4.9%, corresponding to a temporary deployment of approximately 95.1% of the buffer, and then returns toward baseline as the shock variable subsides.

Panel B should be read as a pointwise diagnostic of the trigger rule rather than as a stateful inventory path for remaining buffer capital. The sharp dip immediately after the forced jump is the mathematically expected response of the control law when $\alpha = 100$, $N = 0.5$, and the realized price shock is approximately 38.8%: the rule temporarily deploys about 95.1% of the buffer, leaving about 4.9% undeployed at the peak response. This is an intentionally adversarial stress-test operating point, not a claim about routine market conditions. The relevant structural result is that, even at this extreme point, the policy remains bounded away from one-shot total depletion, and the policy-implied undeployed share mechanically returns toward 100% as the shock dissipates.

5.2 Experiment 2: Historical Backtest and Capital Efficiency

Experiment 2 evaluates the HLCP architecture via an empirical backtest against real-world market data. While theoretical frameworks often evaluate LVR in isolation, net LP profitability relies on the trade-off between accumulated swap fees and realized LVR. Therefore, we map the continuous LVR mechanics directly onto the historical price trajectory and empirical fee generation of the Ethereum mainnet.

5.2.1 Rationale for V2 Empirical Baseline

To ground the backtest, we use a *Uniswap* V2 baseline rather than concentrated-liquidity designs such as Uniswap V3. Equation (1) is derived for a uniform CPMM exposure profile, whereas concentrated liquidity introduces endogenous range selection and path-dependent exposure. Using V2 therefore provides the cleanest control case for isolating the effect of lower active exposure; extending the analysis to concentrated-liquidity ranges is left for future work.

5.2.2 Methodology and the Conservative Worst-Case Assumption

To avoid notation drift, we reserve r_c for the annualized collateral yield rate in Section 4.3 and $Y_C(T)$ for realized collateral yield over a finite horizon T ; in the present backtest, $Y_C(T) = 0$. To construct the evaluation environment, we use the daily closing prices of Ethereum (ETH) throughout 2025, which imply a realized annual volatility of $\sigma \approx 74.56\%$. Concurrently, we extract fee generation from the 2025 Uniswap V2 USDC/ETH pool to establish the benchmark trading environment. The empirical on-chain data imply an average TVL of approximately \$31.21 million and an average daily trading volume of approximately \$3.15 million, corresponding to annual fee revenue of approximately \$3.45 million under the V2 fixed 0.3% fee tier. For the benchmark LP, this implies a gross APR of 11.04% and an effective APY of 11.67%.

We simulate two LP positions over this historical path: a standard V2 CPMM with 100% active capital exposure, and an HLCP with an active scaling factor of $N = 0.5$. To isolate the architectural performance, we assume a 0% external yield on the HLCP's dormant collateral buffer ($Y_C(T) = 0$). This establishes a conservative worst-case scenario in which the buffer generates no auxiliary revenue.

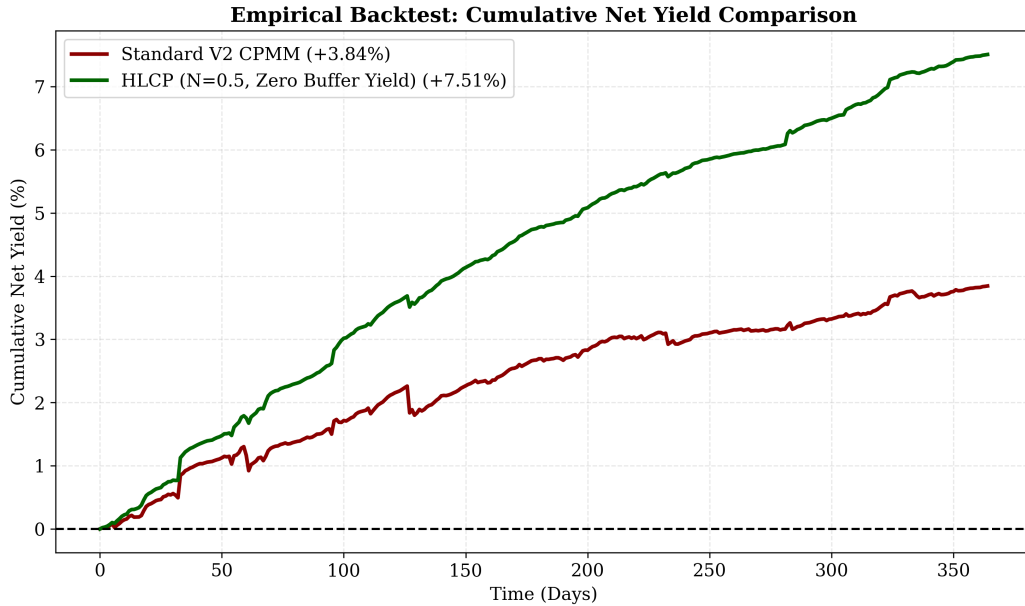
5.2.3 Observations on Net Yield under Reduced Active Exposure

Building upon the adversarial SVJ stress path in Section 5.1, we next evaluate long-horizon profitability on the 2025 ETH path. The cumulative trajectories in Fig. 3 show that the standard Uniswap V2 CPMM experiences substantial LVR drag despite earning the benchmark gross fee APR of 11.04%. By contrast, the HLCP backtest applies the stylized routing assumption introduced in Section 4.3: for routine flow in saturated markets, the router-tolerance condition $\Delta S \leq \varepsilon_{\text{router}}$ is treated as sufficient for benchmark-level fee capture, while only the active fraction $N = 0.5$ remains exposed to LVR.

Under the zero-yield assumption ($Y_C(T) = 0$), the benchmark CPMM ends the sample at a final net yield of +3.84%, whereas the HLCP ends at +7.51%. This is a net-yield improvement of +3.66 percentage points on the sample path. We interpret this result narrowly: under the historical path and the stylized routing assumption used here, lower active exposure improves realized net LP performance even without auxiliary buffer yield.

6 Conclusion and Future Work

This paper studies the Hybrid Liquidity-Collateral Pool (HLCP), a stylized redesign of automated market making in which only a fraction of capital remains continuously exposed to the active constant-product curve. The central observation is geometric: in a CPMM, execution slippage and marginal-price deviation are distinct objects, and the latter remains the relevant quantity for adverse selection. This motivates separating benchmark execution



■ **Figure 3** Empirical backtest of cumulative net yield over the 2025 Ethereum price trajectory. Both the standard V2 CPMM and the HLCP are evaluated under the same benchmark gross-fee assumption; the difference arises from lower active exposure to realized LVR in the HLCP case. The HLCP path is shown for $N = 0.5$ and $Y_C(T) = 0$.

depth from active capital exposure and introducing a trigger-based collateral policy that reacts to economically meaningful price deviations.

Within this modeling framework, the analysis supports three bounded conclusions. First, beyond the saturation region identified in Section 4.1, adding further physical liquidity yields sharply diminishing execution benefits while preserving LVR exposure. Second, under the protocol-enforced control law in Section 4.2, collateral injection remains bounded away from one-shot total exhaustion for any finite shock. Third, in the stylized routing game of Section 4.3 and in the 2025 Uniswap V2 backtest of Section 5, reducing active exposure can improve net LP outcomes even under the conservative assumption $Y_C(T) = 0$.

These conclusions should be interpreted at the level of the model used here. The routing layer is stylized, the backtest uses a uniform V2 baseline rather than concentrated liquidity, and the stress experiment is best understood as a controlled mechanism test rather than a market-complete calibration exercise. Future work should therefore study endogenous router behavior, richer jump calibration, and extensions of the HLCP mechanism to concentrated-liquidity settings such as Uniswap V3.

References

- 1 Austin Adams, Ciamac C Moallemi, Sara Reynolds, and Dan Robinson. am-amm: An auction-managed automated market maker. In *International Conference on Financial Cryptography and Data Security*, pages 93–108. Springer, 2025.
- 2 Hayden Adams, Noah Zinsmeister, Moody Salem, River Keefer, and Dan Robinson. Uniswap v3 core. *Tech. rep., Uniswap, Tech. Rep.*, 2021.
- 3 David S Bates. Jumps and stochastic volatility: Exchange rate processes implicit in deutsche mark options. *The Review of Financial Studies*, 9(1):69–107, 1996.

- 4 Fischer Black and Myron Scholes. The pricing of options and corporate liabilities. *Journal of political economy*, 81(3):637–654, 1973.
- 5 Álvaro Cartea, Fayçal Drissi, and Marcello Monga. Predictable losses of liquidity provision in constant function markets and concentrated liquidity markets. *Applied Mathematical Finance*, 30(2):69–93, 2023.
- 6 T-H. Hubert Chan, Ke Wu, and Elaine Shi. Mechanism Design for Automated Market Makers. In Zeta Avarikioti and Nicolas Christin, editors, *7th Conference on Advances in Financial Technologies (AFT 2025)*, volume 354 of *Leibniz International Proceedings in Informatics (LIPIcs)*, pages 7:1–7:22, Dagstuhl, Germany, 2025. Schloss Dagstuhl – Leibniz-Zentrum für Informatik. URL: <https://drops.dagstuhl.de/entities/document/10.4230/LIPIcs.AFT.2025.7>, doi:10.4230/LIPIcs.AFT.2025.7.
- 7 CoW Protocol. CoW Swap: A fully permissionless trading protocol. <https://cow.fi/cow-swap>, 2026. Accessed: 2026-04-30.
- 8 Philip Daian, Steven Goldfeder, Tyler Kell, Yunqi Li, Xueyuan Zhao, Iddo Bentov, Lorenz Breidenbach, and Ari Juels. Flash boys 2.0: Frontrunning in decentralized exchanges, miner extractable value, and consensus instability. In *2020 IEEE symposium on security and privacy (SP)*, pages 910–927. IEEE, 2020.
- 9 GammaSwap Labs. GammaSwap documentation. <https://docs.gammaswap.com/>, 2026. Accessed: 2026-04-30.
- 10 Hayden et al. Uniswap v2 core. Available at: <https://uniswap.org/whitepaper.pdf>, 2020. (accessed Feb 05, 2025).
- 11 Bence Ladóczk, Miklós Rásonyi, and János Tapolcai. Where does mev really come from? revisiting cexdex arbitrage on ethereum, 2026. URL: <https://arxiv.org/abs/2604.15973>, arXiv:2604.15973.
- 12 Jason Milionis, Ciamac C. Moallemi, Tim Roughgarden, and Anthony Lee Zhang. Automated market making and loss-versus-rebalancing, 2024. URL: <https://arxiv.org/abs/2208.06046>, arXiv:2208.06046.
- 13 Joey Santoro, t11s, Jet Jadeja, Alberto Cuesta Cañada, and Seco. Eip-4626: Tokenized vault standard. Ethereum Improvement Proposals, no. 4626, December 2021. URL: <https://eips.ethereum.org/EIPS/eip-4626>.
- 14 Zhenhang Shang, Zhenyu Zhao, and Kani Chen. Pvpamm: A perpetual market for unbalanced long-short positions. In *7th Conference on Advances in Financial Technologies (AFT 2025)*, pages 34–1. Schloss Dagstuhl–Leibniz-Zentrum für Informatik, 2025.
- 15 Srisht Fateh Singh, Reina Ke Xin Li, Samuel Gaskin, Yuntao Wu, Jeffrey Klinck, Panagiotis Michalopoulos, Zissis Poulos, and Andreas Veneris. Modeling Loss-Versus-Rebalancing in Automated Market Makers via Continuous-Installment Options. In Zeta Avarikioti and Nicolas Christin, editors, *7th Conference on Advances in Financial Technologies (AFT 2025)*, volume 354 of *Leibniz International Proceedings in Informatics (LIPIcs)*, pages 6:1–6:23, Dagstuhl, Germany, 2025. Schloss Dagstuhl – Leibniz-Zentrum für Informatik. URL: <https://drops.dagstuhl.de/entities/document/10.4230/LIPIcs.AFT.2025.6>, doi:10.4230/LIPIcs.AFT.2025.6.